J Solid State Electrochem (2005) 9: 247–253
DOI 10.1007/s10008-004-0598-6

ORIGINAL ARTICLE

Choong Kyun Rhee · Changhoon Jung · Bonseong Ku

2-Dimensional atomic arrangements of Te on Pt(111) whose coverage is higher than 0.25+

Received: 18 August 2004 / Revised: 20 September 2004 / Accepted: 28 September 2004 / Published online: 10 December 2004

Abstract Presented is an in-situ electrochemical STM study on the structural evolution of Te layer on Pt(111) whose coverage is higher than 0.25. The irreversibly adsorbed oxygenated Te layer was reduced to a rectangular $(2\times\sqrt{3})$ adlayer of elemental Te ($\theta_{Te}=0.25$). As additional Te was deposited underpotentially onto the Te-covered Pt(111) surface in a TeO_2-saturated 0.05 M H_2SO_4 solution, the surface structure of Te evolved from the rectangular $(2\times\sqrt{3})$ ($\theta_{Te}=0.25$) to a rectangular $c(2\times\sqrt{3})$ ($\theta_{Te}=0.50$) via a rectangular $c(3\times\sqrt{3})$ ($\theta_{Te}=0.33$). The adsorbed elemental Te was mobile enough to compress the superlattice structure to denser ones, so that the resulting Te layer became electrochemically inactive in the potential range below 0.55 V.

Keywords Single crystal · Pt(111) · Tellurium · Irreversible adsorption · STM

Introduction

Modification of electrode surfaces with foreign metal monolayers is important in manipulating the chemical properties of the surfaces. Electrochemical deposition of a metal monolayer can be achieved in two ways: underpotential deposition [1] and immersion method [2, 3]. In underpotential deposition, metal ions in a solution are reductively deposited onto an electrode surface and the deposited elemental atoms are oxidatively stripped into the solution phase, in general. However, a few elements like Te on Au electrodes, as demonstrated by Stickney [4–8], can be reductively stripped as well. In immersion method, on the other hand, an oxygenated metal ion layer is formed via irreversible adsorption during a contact with a solution containing the metal ions, and the oxygenated layer is reduced electrochemically. Stripping of the oxygenated metal layer into a solution is conducted by oxidation to a soluble species of higher oxidation state. In addition, a redox process is generally observed between the irreversibly adsorbed oxygenated metal ion layer and the corresponding elemental layer as confirmed with an XPS measurement of Te on Pt(111) [9].

Modification of platinum electrodes with irreversible deposition have been aimed to the enhancement in the catalytic activities of modified electrode surfaces toward small organic molecules like methanol and formic acid [10–36]. For example, Ru and Os via immersion method on Pt(111) enhanced greatly the catalytic activity toward methanol oxidation at 0.4 V *vs*. RHE [33, 34]. Furthermore, it has been verified that modification of platinum electrodes with Ru, Os and Ir, i.e. quaternary catalyst, showed the highest activity in methanol oxidation so far [37]. The modifying elements have been known to form nanoislands (2–5 nm in diameter) [33, 34, 38, 39] and to be surface oxides at the potential where the catalytic activity is maximum without being stripped [40, 41]. The roles of the modifying elements in the enhancement of catalytic activity, however, are not understood clearly at atomic level.

Another aspect of irreversible adsorption is formation of metallic layer itself. Recently, our group has published that the two conceptually different processes (underpotential deposition and irreversible adsorption) co-operate to achieve an Sb layer of full coverage on Au(111) and Au(100) [42]. Specifically, an Sb layer of 0.33 monolayer was obtained via irreversible adsorption, and an additional amount of Sb, corresponding to 0.11 monolayer, was deposited sequentially and underpotentially from an Sb-containing solution to result in a

Dedicated to Professor György Horányi, Hungary, on the occasion of his 70th birthday.

C. K. Rhee (✉) · C. Jung · B. Ku
Department of Chemistry, Chungnam National University, Daejun, 305-764, South Korea
E-mail: ckrhee @cnu.ac.kr
Tel.: +82-42-8215483
Fax: +82-42-8231360

full monolayer of Sb. A similar phenomenon has been proposed in the case of Te deposition on Au(111), studied with ex-situ UHV experiments [43] and in-situ EQCM work [44], that a preadsorbed layer of $HTeO^{2+}$ is reduced to show the first under potential deposition peak, followed by the second underpotential one of $HTeO^{2+}$ from solution.

Here, we are presenting an extended in-situ STM study on Te on Pt(111), whose coverage is higher than 0.25. Onto the Pt(111) surface saturated with the oxygenated Te species, whose coverage was 0.25, additional amounts of Te were deposited underpotentially from a Te-containing solution. The structural evolution of the resulting Te layers is discussed in terms of compressed Te layers, concerning their voltammetric behaviors.

Experimental

The Pt(111) single crystal electrodes used in this work were made exclusively by the bead method [45]. A Pt wire (diameter = 0.5 mm, Aldrich, 99.99%) was melt in a hydrogen-oxygen flame to form a platinum single crystal bead, and the orientation of the bead was confirmed with a He-Ne laser. In STM experiments, a single crystal bead was spot-welded on a platinum foil (Johnson Matthey Co., 99.9%) for one of the facets of (111) to be directed to an STM tip. The platinum foil with a single crystal bead was inserted into a home-made electrochemical cell for an STM instrument (Nanoscope III, Digital Instruments). In voltammetric experiments, however, one of the (111) facets was cut and polished to be mirror-like, and the meniscus position was maintained. Annealing in a hydrogen flame and quenching in a hydrogen-saturated water led to well-ordered and clean Pt(111) electrode surfaces in both experiments.

W tips (diameter = 0.25 mm, Aldrich) for STM experiments was fabricated by electrochemical etching in 1 M KOH solution with 15 V AC and coated with a nail polish to minimize electrochemical currents. The scanner used in this work was calibrated with an HOPG crystal (Structure Probe, Inc., USA).

The solutions used in this work were made with ultrapure water (>18 MΩ cm^{-1}, Barnsted), H_2SO_4 (Merck, Suprapur) and TeO_2 (Aldrich, 99.9995%). Especially, the Te solution was obtained by saturating 0.05 M H_2SO_4 with TeO_2 and the Te concentration in the TeO_2 solution was measured to be approximately 0.14 mM.

Voltammetric studies were performed using a conventional three-electrode system and the potentials vs. an Ag|AgCl reference electrode, 1.0 M, Cl^-. An oxidized platinum wire was used as a reference electrode in the STM experiments and the tip bias voltages were reported as controlled against the oxidized platinum reference electrode (−0.7 V against the employed Ag|AgCl reference electrode).

Results and discussions

Voltammetry of Te on Pt(111)

A well-defined Pt(111) electrode (the thin solid line in Fig. 1a) was immersed into the TeO_2-saturated 0.05 M H_2SO_4 solution, equilibrated with air, for 15 min without any potential control to induce the irreversible adsorption of Te (oxygenated Te(IV)(aq) → oxygenated Te(IV)(ad). Upon rinsing the electrode with water thoroughly to remove any residual Te-containing solution, the electrode was subjected to a cathodic scan in 0.05 M H_2SO_4 solution form open circuit potential (normally −0.68 V) and the voltammogram was obtained as shown in the thick solid line of Fig. 1a. Our previous in-situ STM work [46] revealed that the surface redox couple observed at 0.51 V is due to the following reaction: $TeO^{2+}(ad) + 2H^+(aq) + 4e^- \rightleftarrows Te(ad) + H_2O$ and that the coverage of Te adsorbed by irreversible adsorption (the ratio of the number of Te atoms to that of the surface Pt atoms) is 0.25. An ex-situ XPS measurement [9] recently verified a change in the valence state from Te(0) to Te(IV) in the anodic scan and an involvement of adsorbed oxygen in the surface redox process. In both independent experiments [9, 46], the

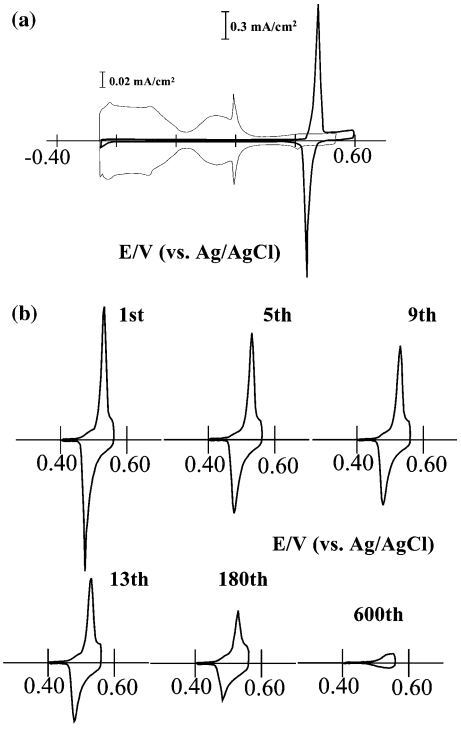

Fig. 1 **a** Cyclic voltammograms of Pt(111) in 0.05 M H_2SO_4 solution after irreversible adsorption in the TeO_2-saturated 0.05 M H_2SO_4 solution for 15 min without any potential control (the thin line represents a voltammogram of a clean and ordered Pt(111)). **b** Cyclic voltammograms of Pt(111) in the TeO_2-saturated 0.05 M H_2SO_4 solution after irreversible adsorption of Te (the numbers of voltammetric cycles are presented). Scan rate: 50 mV s^{-1}

irreversibly adsorbed Te showed a stable voltammetric behavior in the studied potential regions.

A Pt(111) electrode saturated with the adsorbed oxygenated Te showed voltammograms in the TeO_2-saturated 0.05 M H_2SO_4 solution, as in Fig. 1b. The initial voltammogram was identical to that in Fig. 1a. In the subsequent voltammetric cycles, however, the charge related to the redox process of the Te adlayer decreased, and the voltammogram converged ultimately to the one as presented after 30 min voltammetric scan. When the voltammetric scans were interrupted in the TeO_2-saturated 0.05 M H_2SO_4 solution and then resumed in the 0.05 M H_2SO_4 solution, such a decrease of Te charge ceased immediately. These observations clearly indicate that the decrease of Te charge is due to the presence of Te ions in the solution phase. Regardless of voltammetric treatment, the Te layer was stripped oxidatively and irreversibly above 0.55 V. This behavior of the Te adlayer on Pt(111) in a Te-containing solution has been reported by Feliu et al. [47], and a similar phenomenon of the irreversibly adsorbed oxygenous Sb on Pt(111) in an Sb-containing solution has been reported by us [48].

In-situ STM images of Te in atomic scale

In-situ STM was utilized to observe the Te adlayers on Pt(111) along with voltammetric scans in the TeO_2-saturated 0.05 M H_2SO_4 solution. Typical micrographs of atomic arrangements of Te on Pt(111) are shown in Figs. 2, 4 and 5. To obtain the atomic images, a clean and ordered Pt(111) electrode was treated sequentially as follows: (1) contacting a Pt(111) electrode with the TeO_2-saturated 0.05 M H_2SO_4 solution for 15 min without any potential control, (2) rinsing the electrode thoroughly with water, (3) scanning voltammetrically in the TeO_2-saturated 0.05 M H_2SO_4 solution within the potential range between 0.40 and 0.55 V, (4) holding the electrode potential at 0.40 V after voltammetric cycles of a pre-determined number, (5) transferring immediately the electrode covered with the solution drop into an in-situ STM cell and (6) imaging the electrode surface in 0.05 M H_2SO_4 solution under potential control at 0.40 V.

In Fig. 2, two atomic images of Pt(111) covered with Te were observed typically after a voltammetric scan from 0.55 to 0.40 V (a half cycle) in the TeO_2-saturated 0.05 M H_2SO_4 solution. The periodicities among the spots in Fig. 2a are 5.6 ± 0.1 Å and 4.8 ± 0.2 Å along the directions of $[\bar{1}10]$ and $[\bar{1}\bar{1}2]$ respectively, which correspond to 2 and $\sqrt{3}$ times of a Pt-Pt distance (2.77 Å = a). Since the measured angle between the directions of $[\bar{1}10]$ and $[\bar{1}\bar{1}2]$ was close to 90°, the repeating unit in Fig. 2a was assigned to a rectangular (2×√3) pattern as designated at the bottom-middle part in Fig. 2a. Taking the hexagonal symmetry of the Pt(111) substrate into consideration, the rectangular (2×√3) unit cell is equivalent to a c(2×4) repeating unit (see the bottom-left part in Fig. 2a). On the other hand, the repeating unit among

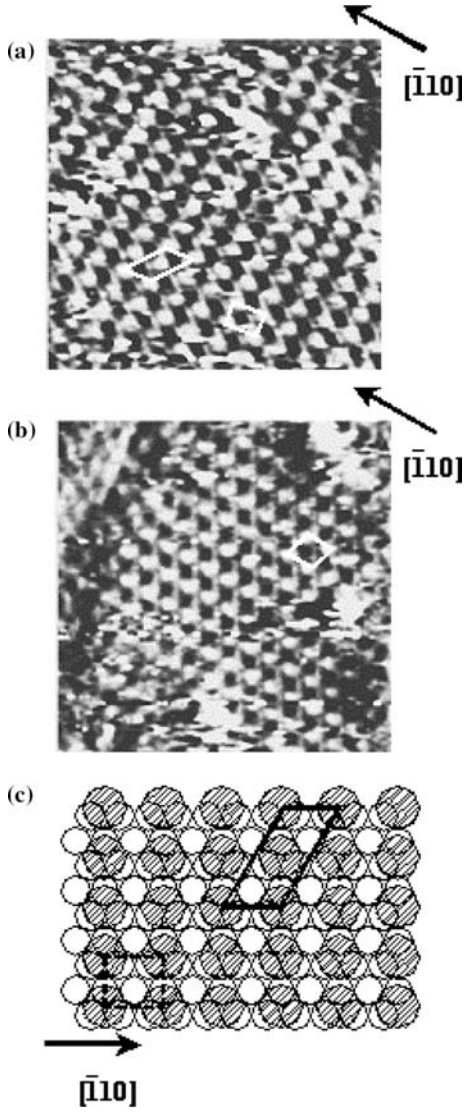

Fig. 2 In-situ STM images of the elemental Te layer of **a** rectangular (2×√3) (or c(2×4)) structure and **b** distorted rectangular (2×√3) structure. All images were observed at 0.40 V in 0.05 M H_2SO_4 solution after a voltammetric scan from 0.55 to 0.4 V (a half cycle) in the TeO_2-saturated 0.05 M H_2SO_4 solution. **c** A schematic model of the rectangular (2×√3) structure (the *open* and *hatched circles* represent Pt and elemental Te atoms, respectively). Tip bias: −575 mV (vs. Pt reference); set point: 51.5 nA; image size: 7 nm

the atomic spots in Fig. 2b, shown at the right-middle part in the image, is not a rectangle but a parallelogram. The dimensions of the parallelogram, however, are identical to those of the rectangular (2×√3) structure in Fig. 2a, so that the Te adlattice as in Fig. 2b was assigned to be a distorted rectangular (2×√3) or distorted c(2×4). Figure 2c is a schematic model for the Te superlattice in Fig. 2a, and the coverage of Te arrayed in the rectangular (2×√3) pattern is 0.25.

It would be interesting to compare this specific rectangular (2×√3) structure of elemental Te (the unit cell drawn with dashed line) with the rectangular (2×√3) structure of irreversibly adsorbed oxygenated Te

(TeO^{2+}) in Fig. 3 (details in reference [43]). Comparison of Fig. 2a with Fig. 3a immediately reveals that the spot density in Fig. 3a is twice higher than that in Fig. 2a. The additional spots in Fig. 3a come from the oxygen atoms at the center of the rectangular (2×√3) unit cell of the oxygenated Te layer (Fig. 3b), while there is no oxygen atom in the rectangular (2×√3) unit cell of the elemental Te layer obtained after electrochemical reduction (Fig. 2c). This contrast indicates that only the oxygen atoms in the adsorbed oxygenated Te species were stripped during reduction. Furthermore, the (8×11) and (2×2) structures of elemental Te, exclusively observed after reduction of the oxygenated Te layer on Pt(111) in 0.05 M H_2SO_4 solution [46], were rarely found after reduction of the oxygenated Te layer in the TeO_2-saturated 0.05 M H_2SO_4 solution. The reason for the absence of the (8×11) and (2×2) structures in this work is not clearly understood.

The micrograph of Fig. 4a was obtained after one and half voltammetric cycles between 0.55 and 0.40 V in the TeO_2-saturated 0.05 M H_2SO_4 solution. Since the separation between the spots was measured to be 4.7 ± 0.1 Å (√3a) and the spots were in a hexagonal symmetry, the repeating unit in Fig. 4a is clearly (√3×√3)R30° (Fig. 4b). The Te coverage of the (√3×√3)R30° structure (0.33) leads quite obviously to the conclusion that more Te was deposited from the TeO_2-saturated 0.05 M H_2SO_4 solution during the additional voltammetric cycle. Fig. 4b shows a schematic of the (√3×√3)R30° structure as well as its equivalent rectangular c(3×√3) structure of square symmetry.

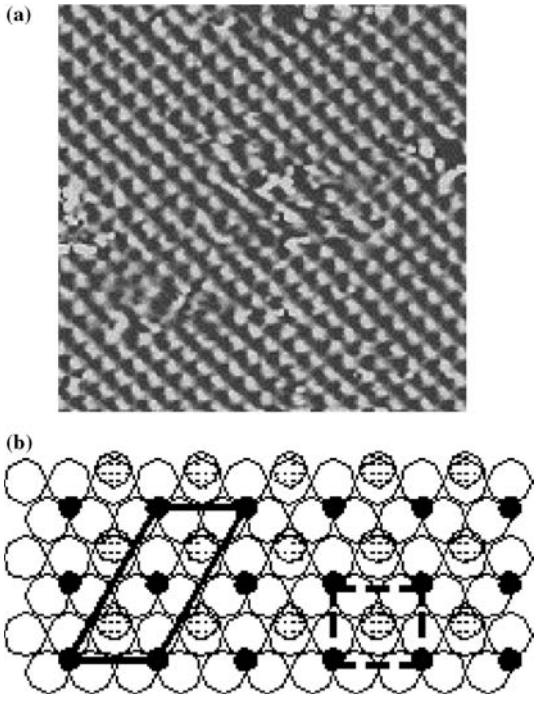

Fig. 3 **a** An in-situ STM image of the irreversibly adsorbed oxygenated Te layer of rectangular (2×√3) (or c(2×4)) structure. The image was observed at 0.55 V in 0.05 M H_2SO_4 solution without any electrochemical treatment. **b** A schematic model of the rectangular c(2×√3) structure (the *open*, *filled* and *hatched circles* represent Pt atom, Te^{4+} and O^{2-} ions, respectively). Tip bias: 770 mV (vs. Pt reference); set point: 26 nA; image size: 7 nm

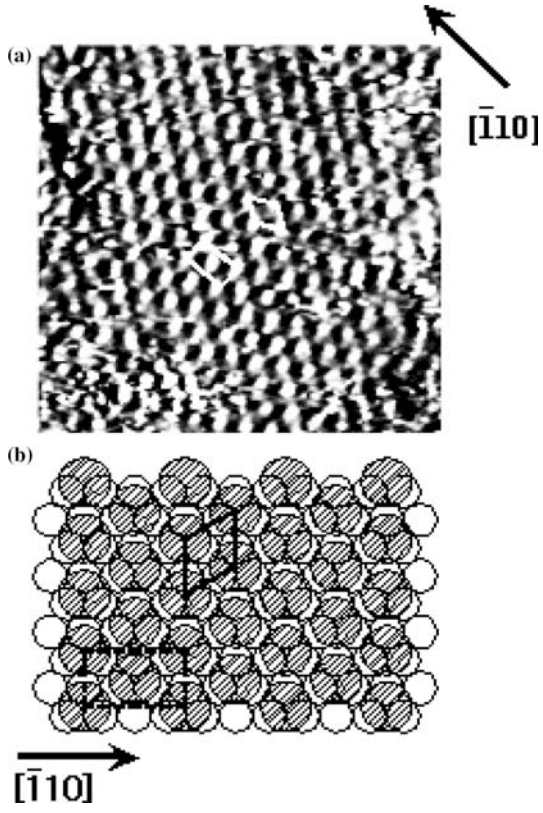

Fig. 4 An in-situ STM image of the elemental Te layer of **a** rectangular c(3×√3) (or (√3×√3)R30°) structure. The image was observed at 0.40 V in 0.05 M H_2SO_4 solution after one and half voltammetric cycles between 0.55 and 0.40 V in the TeO_2-saturated 0.05 M H_2SO_4 solution. **b** A schematic model of the rectangular c(3×√3) structure (the *open* and *hatched circles* represent Pt and elemental Te atoms, respectively). Tip bias: −651 mV (vs. Pt reference); set point: 67 nA; image size: 7 nm

An image of much higher spot density (Fig. 5a) was observed after two and half voltammetric cycles in the TeO_2-saturated 0.05 M H_2SO_4 solution. The atomic row of the highest spot density was found in the $[\bar{1}01]$ direction (45° clockwise from the [110] direction), and the periodicity in the atomic row was 3.7 ± 0.1 Å (√2a). The next densest atomic row was observed in the $[\bar{1}\bar{1}2]$ direction with a frequency of 4.9 ± 0.1 Å (√3a). Based on these values, Te atoms are located on a (1×1) lattice of Pt(111) in c(2×4) (solid line) of hexagonal symmetry or equivalently in rectangular c(2×√3) (dashed line) of square symmetry (Fig. 5b). The Te coverage in the proposed model is 0.5. The in-situ STM results presented so far strongly support that the increase in the coverage of Te on Pt(111) during the voltammetric scans in the TeO_2-saturated 0.05 M H_2SO_4 solution is accompanied with the structural evolution. Another observation to be emphasized is that the structural evolution of Te on Pt(111) was not reversible below 0.55 V at all.

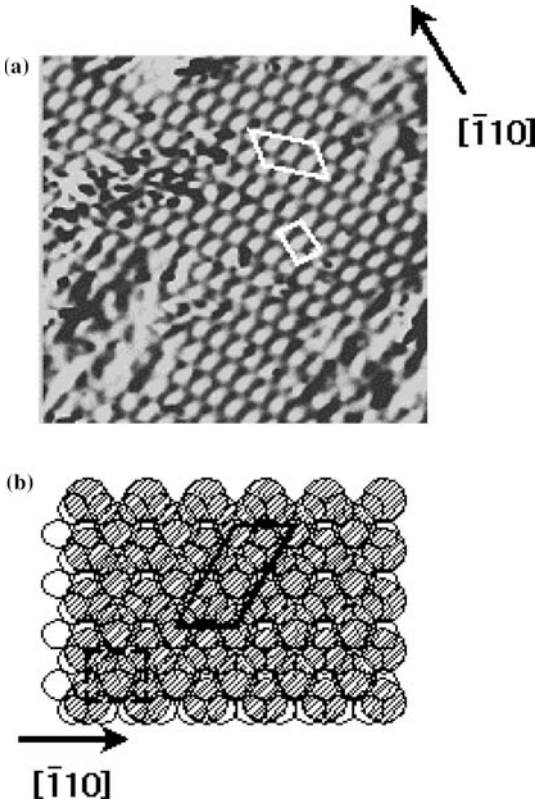

Fig. 5 An in-situ STM image of the elemental Te layer of **a** rectangular c(2×√3) (or c(2×4)) structure. The image was observed at 0.40 V in 0.05 M H_2SO_4 solution after two and half voltammetric cycles between 0.55 and 0.40 V in the TeO_2-saturated 0.05 M H_2SO_4 solution. **b** A schematic model of the rectangular c(2×√3) structure (the *open* and *hatched circles* represent Pt and elemental Te atoms, respectively). Tip bias: −546 mV (vs. Pt reference); set point: 57.9 nA; image size: 7 nm

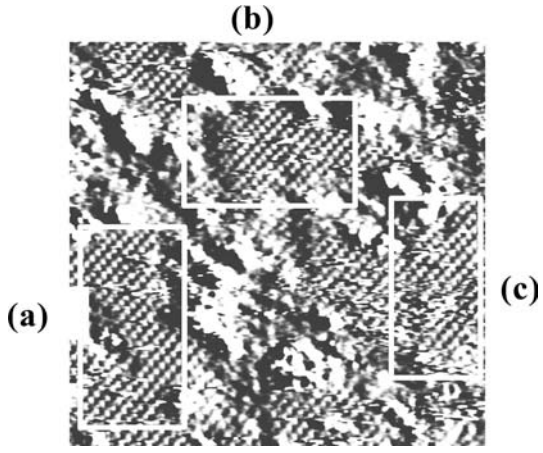

Fig. 6 An in-situ STM image of the elemental Te layer of rectangular c(p×√3) structures: P = **a** 2.5, **b** 2.2 and **c** 2.3. The image was observed at 0.40 V in 0.05 M H_2SO_4 solution after two and half voltammetric cycles between 0.55 and 0.40 V in the TeO_2-saturated 0.05 M H_2SO_4 solution. Tip bias: −509 mV (vs. Pt reference); set point: 81 nA; image size: 18 nm

The structural evolution of the Te layer on Pt(111) during the increase Te coverage would come from the mobility of the deposited elemental Te layer [46]. It is important to notice that there is a space at the center of the rectangular (2×√3) (θ_{Te} = 0.25) unit cell of elemental Te (Fig. 2c), which is occupied by an oxygen atom before reduction (Fig. 3b). If a Te atom is deposited directly into the specific space from the TeO_2-saturated solution, the Te layer of (√3×√3)R30° (Fig. 4b) would not be observed; only the adlattices of the rectangular (2×√3) (θ_{Te} = 0.25) and the rectangular c(2×√3) (θ_{Te} = 0.50) would be observed. The presence of the (√3×√3)R30° structure, therefore, strongly supports that the rectangular (2×√3) (θ_{Te} = 0.25) structure of elemental Te was compressed, probably via distorted rectangular (2×√3) structure, to the (√3×√3)R30° (θ_{Te} = 0.33) structure to provide more spaces for the depositing Te from the solution phase. Further Te deposition induces continuously such a compression until the Te layer reaches to the rectangular c(2×√3) (θ_{Te} = 0.50) structure (Fig. 5b), as exampled in Fig. 6. In Fig. 6, there are three atomically resolved Te domains. A detailed analysis revealed that the atomically resolved domains had rectangular c(P×√3) structures, where p is 2.5a (6.8 ± 0.1 Å), 2.2a (6.2 ± 0.1 Å) and 2.3a (6.4 ± 0.1 Å) in Fig. 6a–c, respectively. These particular values are between 2 and 3, which indicates that the domains observed in Fig. 6 were transient structures being compressed along the [$\bar{1}\bar{1}$0] direction from the rectangular c(3×√3) (θ_{Te} = 0.33) (or (√3×√3)R30°) structures to the rectangular c(2×√3) (θ_{Te} = 0.50) (or c(2×4)) structure.

A comparison of Te/Pt(111) with Te/Au(111)

Interesting is a comparison of the results in this work with those obtained on Te/Au(111), reported by Stickney and his coworkers [43, 49]. On Au(111), Te was underpotentially deposited in two separated steps, although a formation of an oxygenated Te layer prior to the Te deposition was proposed to account for the presence of an oxygen Auger signal. A preadsorbed Te oxide layer [43, 44], probably very weakly, was converted to a elemental Te structure of (√3×√3)R30° (θ_{Te} = 0.33) with an array of domain walls in (13×13) periodicity. Further underpotential deposition modified the (√3×√3)R30° domains sequentially to (√3×317) (θ_{Te} = 0.36) and (3×3) (θ_{Te} = 0.44) domains. In such structural changes, a surface roughening (i.e. pit formation) took place and the whole structural transition was exactly reversed during the corresponding oxidative stripping processes.

Comparing these observations with the behavior of Te on Pt(111) as presented in this work, the structural and voltammetric reversibility of Te layers is contrasting: in Te-containing solution, Te on Au(111) showed structural and voltammetric reversibility, while Te on Pt(111) did not at all. On both surfaces, a preadsorbed layer of an oxygenated Te exists. The only difference between the oxygenated Te layers on the surfaces is their adsorption strengths. On Pt(111), the adsorption

strength of the oxygenated Te is so high that the layer can survive even after a thorough rinsing with water, while on Au(111), the oxygenated Te layer is bound so loosely that the layer desorbs with brief rinsing (we have confirmed the desorption of the Te layer experimentally). The strong interaction between the Pt(111) surface and the oxygenated Te layer, or a stable oxygenated Te layer, is attributable to the involvement of adsorbed oxygen atoms in the redox process of the Te layer on Pt(111) [9]. Thus, some spaces to accommodate the incoming oxygen atoms would be needed to form the stable oxygenated Te layer during the oxidation of Te domains on Pt(111). In the case of the rectangular $(2\times\sqrt{3})$ ($\theta_{Te}=0.25$) domain, there is such a space in the middle of the unit cell, so that the Te domain of $(2\times\sqrt{3})$ ($\theta_{Te}=0.25$) shows its oxidation charge below 0.55 V. In the compressed $c(3\times\sqrt{3})$ ($\theta_{Te}=0.33$) and rectangular $c(2\times\sqrt{3})$ ($\theta_{Te}=0.50$) structures, however, there is no space for the incoming oxygen atoms. For the compressed domains of Te to provide the spaces, a portion of the compressed Te domains should desorb at the potential below 0.55 V. If the Te atoms of the compressed domains were not stripped below 0.55 V, there would be no oxidation current of the adsorbed Te. Indeed, the oxidation charge was decreased as the Te layer was compressed, and the stripping of such Te layer started above 0.55 V.

Summary

The Te layer on Pt(111), whose coverage is more than 0.25, was verified to be produced by two processes: irreversible adsorption and underpotential deposition. In the irreversible adsorption, an oxygenated Te layer (TeO^{2+}) was formed and reduced to show a rectangular $(2\times\sqrt{3})$ (or $c(2\times4)$) array of elemental Te in TeO_2-saturated 0.05 M H_2SO_4 solution. Further underpotential deposition of Te onto the Te-covered Pt(111) surface induced an evolution in the Te superlattice structure from the rectangular $(2\times\sqrt{3})$ ($\theta_{Te}=0.25$) to the rectangular $c(2\times\sqrt{3})$ ($\theta_{Te}=0.50$) via the rectangular $c(3\times\sqrt{3})$ ($\theta_{Te}=0.33$). The compressed Te layer would be relevant to the disappearance of the surface redox peaks of irreversibly deposited oxygenated Te, presumably due to an involvement of adsorbed oxygen.

Acknowledgements The authors appreciate the permission of Central Research Facility, Chungnam National University, Korea, to the STM instrument. One of the authors, Bonseong Ku, was supported by the Korean Science and Engineering Foundation (R05-2004-000-10247-0(2004)).

References

1. Adzic RR (1984) Advances in electrochemistry and electrochemical engineering, vol 13. Wiley, New York
2. Janssen MMP, Moolhuysen J (1976) Electrochim Acta 21:861
3. Janssen MMP, Moolhuysen J (1976) Electrochim Acta 21:869
4. Gregory BW, Suggs SW, Stickney JL (1991) J Electrochem Soc 138:1279
5. Gregory BW, Stickney JL (1991) J Electroanal Chem 300:543
6. Suggs DW, Stickney JL (1991) J Phys Chem B 95:10056
7. Suggs DW, Stickney JL (1993) Surf Sci 290:362
8. Suggs DW, Stickney JL (1993) Surf Sci 290:375
9. Zhou WP, Kiblert LA, Kolb DM (2002) Electrochim Acta 47:4501
10. Clavilier J, Fernandez-Vega A, Feliu JM, Aldaz A (1989) J Electroanal Chem 258:89
11. Clavilier J, Fernandez-Vega A, Feliu JM, Aldaz A (1989) J Electroanal Chem 261:113
12. Fernandez-Vega A, Feliu JM, Aldaz A (1989) J Electroanal Chem 258:101
13. Fernandez-Vega A, Feliu JM, Aldaz A, Clavilier J (1991) J Electroanal Chem 305:229
14. Chang SC, Ho Y, Weaver MJ (1992) Surf Sci 265:81
15. Herrero E, Rodes A, Perez JM, Feliu JM, Aldaz A (1993) J Electroanal Chem 350:73
16. Herrero E, Fernandez-Vega A, Feliu JM, Aldaz A (1993) J Electroanal Chem 350:73
17. Herrero E, Franaszczuk K, Wieckowski A (1993) J Electroanal Chem 361:269
18. Herrero E, Feliu JM, Aldaz A (1994) J Electroanal Chem 368:101
19. Kizhakevariam N, Weaver MJ (1994) Surf Sci 310:183
20. Llorca MJ, Feliu JM, Aldaz A, Clavilier J (1994) J Electroanal Chem 376:151
21. Herrero E, Rodes A, Perez JM, Feliu JM, Aldaz A (1995) J Electroanal Chem 93:87
22. Herrero E, Llorca MJ, Feliu JM, Aldaz A (1995) J Electroanal Chem 383:145
23. Herrero E, Llorca MJ, Feliu JM, Aldaz A (1995) J Electroanal Chem 394:161
24. Llorca MJ, Herrero E, Feliu JM, Aldaz A (1995) J Electroanal Chem 373:217
25. Herrero E, Rodes A, Perez JM, Feliu JM, Aldaz A (1996) J Electroanal Chem 412:165
26. Cramm S, Friedrich KA, Geyzers KP, Stimming U, Vogel R (1997) Fresenius J Anal Chem 358:189
27. Ley KL, Liu RX, Pu C, Fan QB, Leyarovska N, Segre C, Smotkin ES (1997) J Electrochem Soc 144:1543
28. Chrzanowski W, Wieckowski A (1998) Catal Lett 50:69
29. Chrzanowski W, Wieckowski A (1998) Langmuir 14:1967
30. Climent V, Herrero E, Feliu JM (1998) Electrochim Acta 44:1403
31. Gurau B, Viswanathan R, Liu RX, Lafrenz TJ, Ley KL, Smotkin ES, Reddington E, Sapienza A, Chan BC, Mallouk TE, Sarangapani S (1998) J Phys Chem B 102:9997
32. Tremiliosi G, Kim H, Chrzanowski W, Wieckowski A, Grzybowska B, Kulesza PJ (1999) Electroanal Chem 467:143
33. Crown A, Kim H, Lu GQ, de Moraes IR, Rice C, Wieckowski A (2000) J New Mater Electrochem Sys 3:275
34. Crown A, de Moraes IR, Wieckowski A (2001) J Electroanal Chem 500:333
35. Macia MD, Herrero E, Feliu JM, Aldaz A (2001) J Electroanal Chem 500:498
36. Macia MD, Herrero E, Feliu JM (2002) Electrochim Acta 47:3653
37. Reddington E, Sapienza A, Gurau B, Viswanathan R, Sarangapani S, Smotkin ES, Mallouk TE (1998) Science 280:1735
38. Crown A, Wieckowski A (2001) Phys Chem Chem Phys 3:3290
39. Crown A, Johnston C, Wieckowski A (2002) Surf Sci 506:L268
40. Kim H, de Moraes IR, Tremiliosi G, Haasch R, Wieckowski A (2001) Surf Sci 474:L203
41. Rhee CK, Wakisaka M, Tolmachev Y, Johnston C, Haasch R, Attenkofer K, Lu GQ, You H, Wieckowski A (2003) J Electroanal Chem 554–555:367
42. Jung G, Rhee CK (1997) J Electroanal Chem 436:277
43. Sorenson TA, Varazo K, Suggs SW, Stickney JL (2001) Surf Sci 470:197

44. Nicic I, Liang J, Cammarata V, Alanyalioglu M, Demir U, Shannon C (2002) J Phys Chem B 106:12247
45. Clavilier J, Faure R, Guinet G, Durand R (1980) J Electroanal Chem 107:205
46. Rhee CK, Kim DK (2001) J Electroanal Chem 506:149
47. Feliu JM, Llorca MJ, Gomez G, Aldaz A (1993) Surf Sci 297:209
48. Jung G, Park H, Rhee CK (1998) J Electroanal Chem 453:243
49. Lay MD, Stickney JL (2004) J Electrochem Soc 151:C431